QUANTITATIVE MICROWAVE TOMOGRAPHY FROM SPARSE MEASUREMENTS USING A ROBUST HUBER REGULARIZER

F. Bai [1]*, A. Pižurica* [1]*, S. Van Loocke* [2]*, A. Franchois* [2]*, D. De Zutter* [2]*, W. Philips* [1]

[1] Department of Telecommunications and Information Processing (IPI-TELIN-IBBT),
[2] Department of Information Technology (INTEC),
Ghent University, Belgium

ABSTRACT

In statistical theory, the Huber function yields robust estimations reducing the effect of outliers. In this paper, we employ the Huber function as regularization in a challenging inverse problem: quantitative microwave imaging. Quantitative microwave tomography aims at estimating the permittivity profile of a scattering object based on measured scattered fields, which is a nonlinear, ill-posed inverse problem. The results on 3D data sets are encouraging: the reconstruction error is reduced and the permittivity profile can be estimated from fewer measurements compared to state-of-the art inversion procedures.

Index Terms— inverse problem, microwave imaging, robust estimation, regularization.

1. INTRODUCTION

Quantitative microwave tomography aims at reconstructing the exact permittivity profile of an unknown scattering object by illuminating the object with microwaves and by measuring the scattered electric field. Different approaches exist for solving this ill-posed nonlinear inverse problem [1–6]. In [1], edge preserving regularization was imposed on the real and imaginary part of the complex permittivity separately. Multiplicative smoothing (MS) [4] applies Tikhonov regularization in a multiplicative fashion. A related, earlier method applies total variation (TV) as a multiplicative constraint [5]. The Value Picking (VP) regularizer [6] favors solutions consisting of piece-wise constant permittivities, without imposing this constraint in a strict sense.

In this paper, we propose a novel reconstruction algorithm using robust statistical regularization. To the best of our knowledge, such approaches were not reported in microwave tomography so far. In particular, we regularize the problem by imposing the Huber robust potential function [7] on the neighboring values of the complex permittivity. The Huber function

$$g_{Huber}(\eta) = \begin{cases} \eta^2 & |\eta| \leq \gamma \\ 2\gamma|\eta| - \gamma^2 & else \end{cases} \quad (1)$$

is quadratic for small values of η and linear for large values, avoiding in this way over-smoothing at true discontinuities. Related robust methods are used extensively in vision applications, such as image restoration, segmentation, surface and shape filling and pose estimation [7]. Recently, a related Huber Markov Random Field regularizer was employed in SAR imaging [8] and in parallel magnetic resonance imaging [9]. These are however linear inverse problems, while the problem considered in this paper is non-linear and involves different physical and computational mechanisms. We derive a reconstruction algorithm where a Huber function with a complex argument regularizes the non-linear cost function, which is then optimized by a modified Gauss-Newton technique.

Our experiments demonstrate a significant improvement over the recent related methods in microwave tomography. The profiles are reconstructed more accurately and the advantages are especially prominent when the measurements are sparse. In Section 2 the electromagnetic inverse scattering problem and Gauss-Newton method are revisited. The proposed Huber regularization is discussed in Section 3 and results on 3D datasets are presented in Section 4. Section 5 concludes the paper.

2. PROBLEM FORMULATION

Consider an unknown object with complex permittivity $\boldsymbol{\varepsilon}(\mathbf{r})$ embedded in free space $\boldsymbol{\varepsilon}_0$ that is illuminated successively with different known time-harmonic incident fields. The discretized unknown permittivity profile $\boldsymbol{\varepsilon}$ is estimated iteratively, on a grid with N^{ε} square (2D) or cubic (3D) cells within a reconstruction domain $\mathcal{D}$, alternating between the forward and the update problem. The forward problem simulates the scattered electric field for a guessed permittivity profile, using a volume integral equation (VIE) [6]. The scattered fields $\mathbf{e}^{scat}(\boldsymbol{\varepsilon})$ collected by a number of receiving antennas in the simulation are compared with the measured fields $\mathbf{e}^{meas}$. Based on the resulting error, the permittivity profile is updated. Typically, the inverse problem is solved by minimizing a cost function

$$F(\boldsymbol{\varepsilon}) = F^{LS}(\boldsymbol{\varepsilon}) + \mu F^{R}(\boldsymbol{\varepsilon}) \quad (2)$$

where $F^{LS}(\boldsymbol{\varepsilon})$ is the least squares cost function, which evaluates the data error and $F^R(\varepsilon)$ is a regularization term, with the parameter $\mu \geq 0$. The least square cost function is

$$F^{LS}(\boldsymbol{\varepsilon}) = \frac{\|\mathbf{e}^{meas} - \mathbf{e}^{scat}(\boldsymbol{\varepsilon})\|^2}{\|\mathbf{e}^{meas}\|^2} \tag{3}$$

where $\mathbf{e}^{meas}$ and $\mathbf{e}^{scat}(\varepsilon)$ are $N^{\mathcal{D}}$-dimensional vectors that contain the data for all combinations of illuminating and receiving antennas.

We consider minimization by an approximate line search along a modified Gauss-Newton direction [6]. The complex permittivity in iteration k is updated as $\boldsymbol{\varepsilon}_{k+1} = \boldsymbol{\varepsilon}_k + \beta_k \boldsymbol{\Delta\varepsilon}_k$, where β_k is caculated from line search [6] and $\boldsymbol{\Delta\varepsilon}_k$ is obtained from

$$(\mathbf{J}_k^H \mathbf{J}_k + \lambda^2 \boldsymbol{\Sigma}_k^R)\boldsymbol{\Delta\varepsilon}_k = -(\mathbf{J}_k^H[\mathbf{e}^{scat}(\boldsymbol{\varepsilon}_k) - \mathbf{e}^{meas}] + \lambda^2 \boldsymbol{\Omega}_k^{R*}) \tag{4}$$

where $(.)^H$ stands for Hermitian transpose and $(.)^*$ denotes the complex conjugate. The trade-off parameter λ is given by $\lambda^2 = \mu\|\mathbf{e}^{meas}\|^2$ [6]. In the following, the subscript k is omitted. $\mathbf{J}$ is the $N^{\mathcal{D}} \times N^{\varepsilon}$ Jacobian matrix, which contains the derivatives of the scattered field components with respect to the optimization variables: $J_{dl} = \partial e_d^{scat}/\partial\varepsilon_l$; $\boldsymbol{\Omega}_k^{R*}$ is an $N^{\varepsilon}-$dimensional vector that contains the derivatives of the regularizing function, $\Omega_l^{R*} = \partial F^R/\partial\epsilon_l^*$; $\boldsymbol{\Sigma}^R$ is a $N^{\varepsilon} \times N^{\varepsilon}$ matrix, $\Sigma_{l,l'}^R = \partial^2 F^R/\partial\epsilon_l\partial\epsilon_{l'}^*$. The factor $\mathbf{J}^H\mathbf{J} + \lambda^2\boldsymbol{\Sigma}^{\mathcal{R}}$ is known as a modified Gauss-Newton Hessian matrix. To avoid ill-conditioning of the forward problems constraints are imposed on the real and imaginary parts of the complex permittivity by a modified, constrained line search.

3. HUBER REGULARIZED RECONSTRUCTION ALGORITHM

In this paper, we define the regularization term $F^R(\boldsymbol{\varepsilon})$ in (2) as follows

$$F^R(\boldsymbol{\varepsilon}) = \frac{1}{2}\sum_l \sum_{l' \in N_l} g_{Huber}(|\varepsilon_l - \varepsilon_{l'}|) \tag{5}$$

with g_{Huber} defined in (1). The index l denotes the spatial position. In 2D, it is a pair of indices $l \equiv (i, j)$ and in 3D a triplet $l \equiv (i, j, k)$. N_l is the neighborhood of l. For the chosen regularization function, we derive $\boldsymbol{\Omega}^{R*}$ and $\boldsymbol{\Sigma}^R$ in (4). Taking into account that ε in (5) is a complex number and hence $|\varepsilon_l - \varepsilon_{l'}|^2 = (\varepsilon_l - \varepsilon_{l'})(\varepsilon_l^* - \varepsilon_{l'}^*)$, it can be shown that

$$\begin{aligned}\Omega_l^{R*} &= \frac{\partial F^R}{\partial \varepsilon_l^*} \\ &= \sum_{l' \in N_l} \begin{cases} (\varepsilon_l - \varepsilon_{l'}) & |\varepsilon_l - \varepsilon_{l'}| \leq \gamma \\ \gamma \dfrac{(\varepsilon_l - \varepsilon_{l'})}{|\varepsilon_l - \varepsilon_{l'}|} & otherwise \end{cases}\end{aligned} \tag{6}$$

Algorithm 1 The complete algorithm for reconstructing $\boldsymbol{\varepsilon}$

Require: $\boldsymbol{\varepsilon}_{init}$, μ, γ
Ensure: Objects, configuration
  $\boldsymbol{\varepsilon}_0 \leftarrow \boldsymbol{\varepsilon}_{init}$
  Measure $\mathbf{e}^{meas}$, compute $\lambda^2 = \mu\|\mathbf{e}^{meas}\|^2$
  repeat
    Compute $\mathbf{e}^{scat}(\boldsymbol{\varepsilon})$
    if $\dfrac{\|\mathbf{e}^{meas} - \mathbf{e}^{scat}(\boldsymbol{\varepsilon})\|^2}{\|\mathbf{e}^{meas}\|^2} < 10^{-3}$ **then**
      return $\boldsymbol{\varepsilon}$
    else
      Compute $\mathbf{J}_k$: $J_{dl} = \partial e_d^{scat}/\partial\varepsilon_l$
      Compute $\boldsymbol{\Omega}_k^{R*}$ and $\boldsymbol{\Sigma}_k^R$ using (6-8)
      Compute $\boldsymbol{\Delta\varepsilon}_k$ using (4)
      Compute β_k with line search
      $\boldsymbol{\varepsilon}_{k+1} = \boldsymbol{\varepsilon}_k + \beta_k\boldsymbol{\Delta\varepsilon}_k$
    end if
  until k=The number of maximum iterations
  print $\boldsymbol{\varepsilon}$

We obtain the diagonal elements of $\boldsymbol{\Sigma}^R$ as

$$\begin{aligned}\Sigma_{l,l}^R &= \frac{\partial^2 F^R}{\partial\varepsilon_l\partial\varepsilon_l^*} \\ &= \sum_{l' \in N_l} \begin{cases} 1 & |\varepsilon_l - \varepsilon_{l'}| \leq \gamma \\ \dfrac{\gamma}{2|\varepsilon_l - \varepsilon_{l'}|} & otherwise \end{cases}\end{aligned} \tag{7}$$

and the non-diagonal elements as

$$\begin{aligned}\Sigma_{l,l'}^R &= \frac{\partial^2 F^R}{\partial\varepsilon_{l'}\partial\varepsilon_l^*} \\ &= \begin{cases} -1 & |\varepsilon_l - \varepsilon_{l'}| \leq \gamma \\ -\dfrac{\gamma}{2|\varepsilon_l - \varepsilon_{l'}|} & otherwise \end{cases}\end{aligned} \tag{8}$$

A pseudo-code of the complete reconstruction is given under Algorithm 1. We optimize the regularization parameter μ and the parameter γ of the Huber function experimentally. For piece-wise constant objects $\gamma = 0.1$ is a good choice and for continuous profiles (like in biomedical cases) a smaller γ (0.008) should be used. For the regularization parameter μ we obtained the same optimal value ($\sim 1e-6$) for different targets and different antenna configurations. For the neighborhood N_l we used 26 nearest neighbors in 3D as a compromise between reconstruction quality and complexity.

4. RECONSTRUCTION RESULTS

We performed experiments with different dipole antenna configurations, including the configuration from [6] (shown in Fig. 1(a)) and much sparser configurations, like in Fig. 1(b), (c). The sparser configurations are very attractive from the

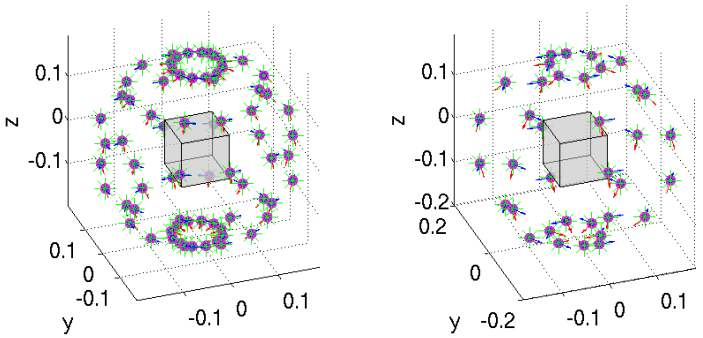

(a) 20376 data points

(b) 5184 data points

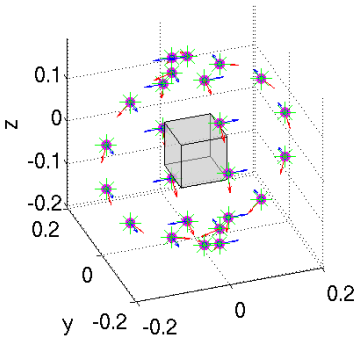

(c) 2304 data points

Fig. 1. Three dipole configurations with antenna positions (dots) on a sphere with radius 0.2m. The arrows in two orthogonal directions indicate transmitting dipoles. The cube in the center indicates the reconstruction domain $\mathcal{D}$.

point of view of computation time but make the reconstruction problem much more challenging.

We compare the reconstruction results with three different regularizations: multiplicative smoothing (MS) [4], step-wise relaxed value picking (SRVP) [6] and the proposed Huber regularization. The Object 1 under investigation is a homogeneous sphere with radius $r_a = 30$mm and relative permittivity $\varepsilon_r = 2$, positioned in the center of the reconstruction grid (see Fig. 2(a)). The Object 2 is a cube with side 22.5mm and permittivity 2.5-1j, which is embedded in a sphere with radius 30mm and permittivity 1.8. The sphere and cube are centered at the origin and at the point (-5.6mm,-5.6mm,-5.6mm), respectively (see Fig. 4(a)). The constraints on the permittivity are $1 < Re(\varepsilon) < 10$, $-10 < Im(\varepsilon) < 0$. The reconstruction domain is a $0.1 \times 0.1 \times 0.1$ m^3 cube and is discretized in $20 \times 20 \times 20$ voxels, with edge size 5 mm, yielding a total of 8000 permittivity unknowns. We use this grid for both forward and update problems as well as for generating the data. We simulate scattered field measurements at 8GHz.

Each dipole in the three configurations is used to illuminate the target and the scattered field is measured in every dipole position and along each dipole direction. The configuration in Fig. 1(a) taken from [6] consists of 144 antennas which generate 20736 complex data points. The configuration in Fig. 1 (b) consists of 36 antennas which generate 5184 data points. The sparsest configuration in Fig. 1 (c) consists of 24 antennas which generate 2304 data points.

Relative error	MS	SRVP	Huber
20736 data points	0.0635	0.0343	0.0151
5184 data points	0.0674	0.0458	0.0206
2304 data points	0.0879	0.1301	0.0332

Table 1. Relative errors in the permittivity estimation of Object 1 for different methods and configurations from Fig. 1.

In our experiments, a stabilized bi-conjugate gradient Fast Fourier Transform (BICGSTAB-FFT [10]) forward solver, which could be parallelized, is used to accelerate the calculations. The computation time is similar for all three considered regularizations provided that equal numbers of antennas are used. The chosen antenna configuration may have a large impact on the computation time. To reconstruct Object 1, the dense configuration from Fig. 1 (a) requires 3 hours while the sparsest configuration from Fig. 1 (c) requires only around 40 minutes on a six-core Intel i7 980x processor (3.33GHz) with 24GByte memory.

The relative error of the reconstruction, defined as $R = \| \hat{\boldsymbol{\varepsilon}} - \boldsymbol{\varepsilon}^{true} \|^2 / \|\boldsymbol{\varepsilon}^{true}\|^2$ where $\hat{\boldsymbol{\varepsilon}}$ denotes the estimated and $\boldsymbol{\varepsilon}^{true}$ the true permittivity profile, is shown in Table 1 for the three antenna configurations. Visual results are shown in Fig. 2, Fig. 4 (Object 1 in Fig. 1 (c)) and in Fig. 2 (Object 2 in Fig. 1 (b)).

The results in Table 1 show that the proposed method with Huber regularization yields best results for all antenna configurations: it yields a smaller relative error than SRVP and MS even with much fewer measurements, reducing thereby drastically the complexity of the system. The SRVP is superior to MS for the dense antenna configuration but does not seem to cope well with sparse measurements. The reconstructed profiles in Fig. 2-Fig. 4 show the improvement visually and demonstrate the potential of the proposed method for reconstruction from sparse measurements. More results for other objects and different antenna configurations in 2D and 3D are available at our website http://telin.ugent.be/∼fbai/MicrowaveTomography/.

5. SUMMARY

In this paper, we have introduced a new algorithm for quantitative microwave tomography using Huber regularization. The results show a significant improvement over recent related methods and indicate potential for efficient reconstruction from sparse measurements. By decreasing the number of required transmitting and receiving antennas, the computation time is drastically reduced.

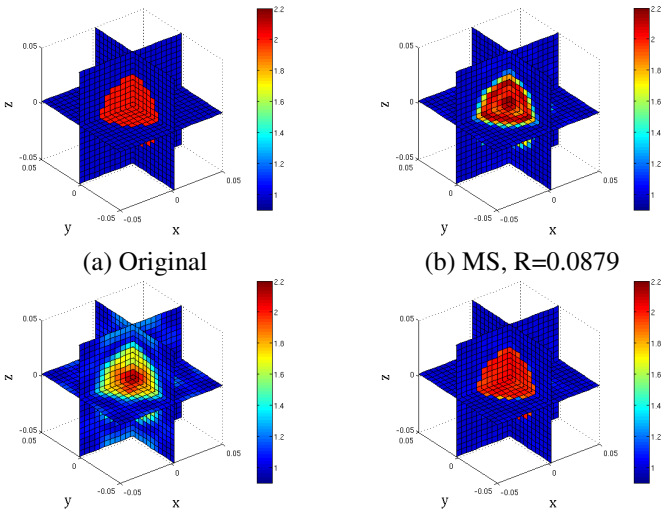

(a) Original (b) MS, R=0.0879

(c) SRVP, R=0.1301 (d) Huber, R=0.0332

Fig. 2. Real parts of the complex permittivity profile for Object 1 (see text) and antenna configuration from Fig. 1 (c).

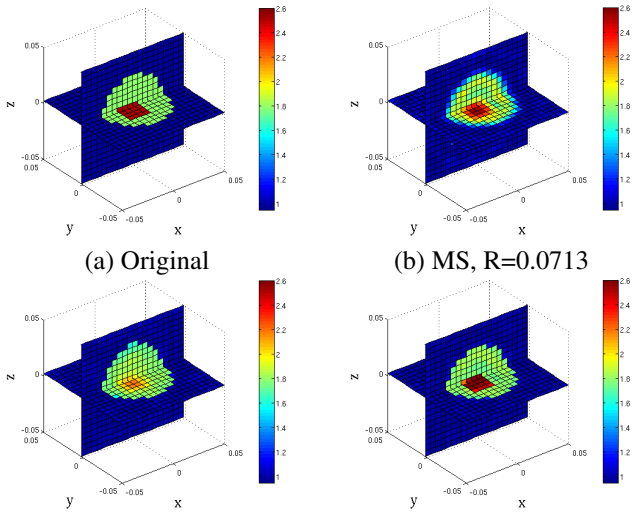

(a) Original (b) MS, R=0.0713

(c) SRVP, R=0.0734 (d) Huber, R=0.0259

Fig. 4. Real parts of the complex permittivity profile for Object 2 (see text) and antenna configuration from Fig. 1 (b).

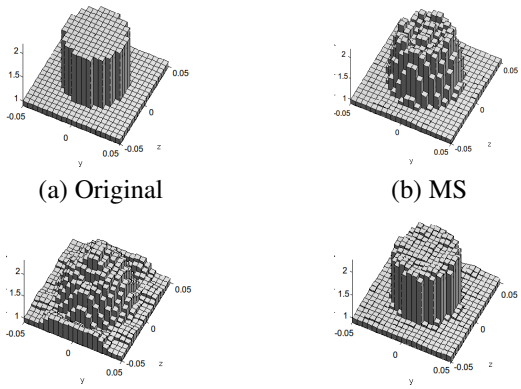

(a) Original (b) MS

(c) SRVP (d) Huber

Fig. 3. Cross-sections of the corresponding permittivity profiles from Fig. 2.

References

[1] P. Lobel, C. Pichot, L. Blanc-Feraud, and M. Barlaud, "Microwave imaging: Reconstructions from experimental data using conjugate gradient and enhancement by edge-preserving regularization," *Int. Journal of Imaging Syst. and Technol.*, vol. 8, no. 4, pp. 337–342, 1997.

[2] A. Fhager, M. Gustafsson, and S. Nordebo, "Image reconstruction in microwave tomography using a dielectric Debye model," *IEEE Trans. Biomed. Eng.*, vol. 59, no. 1, pp. 156 –166, Jan 2012.

[3] M. Lazebnik, D. Popovic, L. McCartney, and C. Watkins, "A large-scale study of the ultrawideband microwave dielectric properties of normal, benign and malignant breast tissues obtained from cancer surgeries," *Physics in Med. and Biol.*, vol. 52, no. 20, pp. 6093–6115, 2007.

[4] J. De Zaeytijd and A. Franchois, "Three-dimensional quantitative microwave imaging from measured data with multiplicative smoothing and value picking regularization," *Inverse Probl.*, vol. 25, no. 2, pp. 024004, 2009.

[5] A. Abubaker and P.M. Van Den Berg, "Total variation as a multiplicative constraint for solving inverse problems," *IEEE Trans. Image Process.*, vol. 10, no. 9, pp. 1384 –1392, Sep 2001.

[6] J. De Zaeytijd, A. Franchois, and J.M. Geffrin, "A new value picking regularization strategy - application to the 3-D electromagnetic inverse scattering problem," *IEEE Trans. Antennas Propag.*, vol. 57, no. 4, pp. 1133 –1149, April 2009.

[7] Stan Z. Li, *Markov Random Field Modeling in Image Analysis*, Springer, 1995.

[8] M. Soccorsi, D. Gleich, and M. Datcu, "Huber-Markov model for complex SAR image restoration," *IEEE Geosci. Remote Sens. Lett.*, vol. 7, no. 1, pp. 63 –67, Jan 2010.

[9] L. Ying, B. Liu, M. C. Steckner, G. Wu, M. Wu, and S. Li, "A statistical approach to SENSE regularization with arbitrary k-space trajectories," *Magnetic Resonance in Medicine*, vol. 60, no. 2, pp. 414–421, 2008.

[10] H. A. van der Vorst, "Bi-cgstab: a fast and smoothly converging variant of bi-cg for the solution of nonsymmetric linear systems," *SIAM J. Sci. Stat. Comput.*, vol. 13, no. 2, pp. 631–644, Mar. 1992.